Journal of Computational Physics **166,** 152–158 (2001)
doi:10.1006/jcph.2000.6642, available online at http://www.idealibrary.com on IDEAL®

NOTE

On Thin Shear Layers Numerical Simulation

A. I. Tolstykh and E. N. Chigirev

Computing Center of Russian Academy of Sciences, Moscow Vavilova str. 40, Russia
E-mail: tol@ccas.ru, chiger@ccas.ru

Received April 26, 1999; revised April 26, 2000

Key Words: Navier–Stokes equations; incompressible flows; vorticity–stream function formulation; shear layer; compact upwind differencing.

1. In [1, 2], very instructive results concerning the ability of different numerical methods to resolve properly unstable thin shear layers described by the incompressible Navier–Stokes equations were presented. An interesting aspect of the studies was the scheme-induced artifact that manifested in the form of spurious vortices when the meshes used in the calculations seemed to be quite refined giving the impression that the solutions were mesh-converged. It was shown that further refining of meshes removed these artifacts completely and gave "true" solutions to the problem.

From [1, 2], a question may arise concerning the mesh size needed to get the "true" solution for given input data and its dependence on the methods used in the calculations. The results presented in [1, 2] show that though the performances of the tested methods may differ (especially in comparisons of centered and upwind schemes), meshes sufficient in most cases for the resolution of stable oscillation-free solutions are about the same for fixed input data. In this note, we try to show that the number of grid points in the computational domain needed to resolve thin shear layers properly can be considerably decreased (at least by a factor of 4) when more accurate schemes are used. Other aims are to enlarge the "database" of scheme performances presented in [1, 2] and add new observations based on high-accuracy calculations.

2. We consider the double-periodic problems of [1, 2], namely the roll-up of the shear layers given initially by the Cartesian velocities

$$u = \tanh(\rho(y - 0.25)) \quad \text{for } y \le 0.5, \qquad \tanh(\rho(0.75 - y)) \quad \text{for } y > 0.5 \tag{1}$$

$$v = \delta \sin(2\pi x) \tag{2a}$$

$$v = \delta \sin(2\pi(x + 0.25)), \tag{2b}$$

where (2a) and (2b) are the initial perturbations used in [1] and [2], respectively.

0021-9991/01 $35.00

The incompressible Navier–Stokes equations written in the vorticity–stream function form (ω–ψ) were discretized in the following manner. For convective terms, the fifth-order compact upwind differencing (CUD-II-5) described in [3] was used while the fourth-order compact formulas were applied to the second derivatives in the viscous terms and the Laplace operator in the Poisson equation. The velocity components were also discretized using the fourth-order compact differencing for ψ. Though its overall order is 4, the scheme differs from the conventional fourth-order schemes considered in [1, 2] in that it contains very small numerical constants in its truncation errors, especially in those for nonlinear terms. Besides, using CUD allows one to obtain with great ease arbitrary Reynolds number oscillation-free thin layer solutions for coarse and fine meshes without adding artificial dissipation mechanisms apart from the built-in fifth-order CUD dissipation.

Though the important point in the thin layers problems seems to be the spatial discretizations, high-order time-stepping methods were used in the present calculations. They were the fourth-order Runge–Kutta method and the newly proposed highly accurate fifth-order time integrator [4] applicable to hyperbolic and parabolic PDE and stiff ODE systems. Figure 1 shows the CUD L_1-norms of the solution errors versus grid point numbers for the travelling wave exact solution presented in [2]. For comparison, the most accurate results obtained in [2] via difference techniques (by using the fourth-order centered scheme for the ω–ψ formulation), as well as via the pseudospectral method, are also shown. As can be seen, the accuracy of the CUD method is intermediate between those of the difference and the pseudospectral methods used in [2], but the convergence order is the highest.

The calculations were carried out for input data identical to those of [1] [$\rho = 100$, Re $=$ 1/20,000, initial perturbation (2a) with $\delta = 0.05$] and [2] [$\rho = 80$, Re $= 1/10{,}000$, initial perturbation (2b) with $\delta = 0.05$] and had approximately the same meshes. They will be referred to as Cases A and B, respectively.

In [1], the spurious vortex (say, at $t = 0.8$) is seen in the case of 256×256 mesh but disappears when the 512×512 mesh is used. The vorticity contours of the present

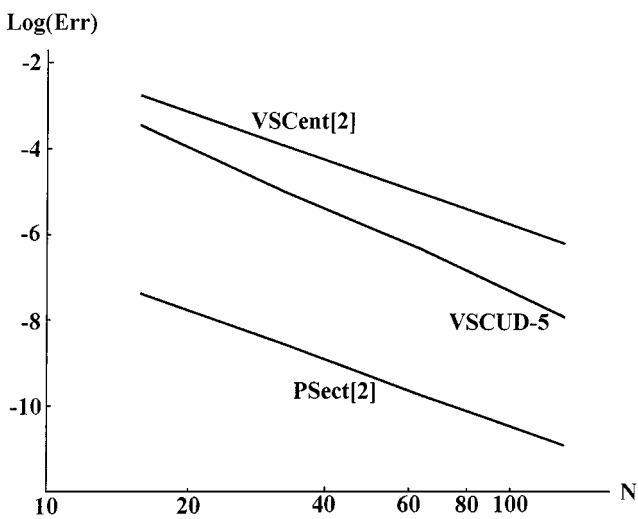

FIG. 1. Convergence curves for the travelling wave example of [2]: L_1 norms of the velocity u errors (Err) vs number of grid points (N). The computed convergence rates are (from top to bottom) fourth-order centered scheme [2] (VScent): 4.01 [2], present (CUD-II-5): 4.94, and pseudospectral [2] (PSpect): 4.00 [2].

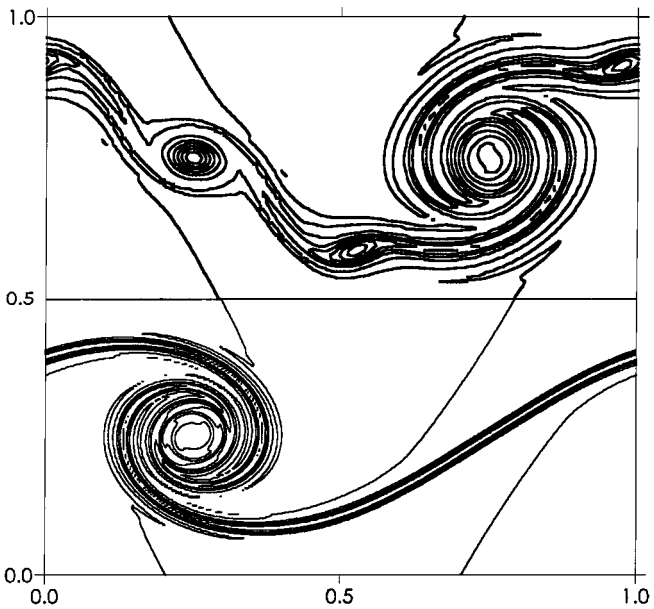

FIG. 2. Removing spurious vortex by refining meshes: vorticity contours for the thin layer example of [1] (Case A). The meshes are 129×129 (top) and 257×247 (bottom).

calculations corresponding to the same time moment are shown in Fig. 2 for 127×127 mesh (top) and 257×257 mesh (bottom). They are indiscernible from those of [1] though they were obtained with meshes two times coarser. The results for Case B (not presented here) show the same tendency. For example, when the robust methods are compared, the 127×127 mesh rather than the 256×256 mesh of [2] suffices to provide artifact-free mesh-converged solutions without any evidence of spurious oscillations.

3. To add new information to that presented in [1, 2], inviscid solutions were calculated for the above-mentioned cases by setting $\mathrm{Re} = \infty$. The reasons are as follows. In the present double-periodic case, the viscous terms can be considered as non-singular perturbations to the Euler equations (this is not true when solid boundaries are encountered). By neglecting them, one can clearly see the vorticity-production capabilities of discrete non-linear terms. When this is done, there is no loss of essential flow features, since viscous patterns simply mimic inviscid ones.

Figures 3 and 4 show the vorticity isolines at $t = 0.8$ and $t = 1.0$ corresponding to the inviscid analogues of Cases A and B, respectively, using under-resolving (top) and well-resolving (bottom) meshes. From these figures, two conclusions may be drawn.

First, artifacts in the form of three spurious vortices do exist in the inviscid case calculated by the present method with relatively coarse meshes.

Second, in comparison with the viscous case, more refined meshes are needed to remove them completely, that is, 513×513 and 257×257 for the input parameters of Cases A and B, respectively.

The results upon which the first conclusion is based add some new information to that presented in [1, 2]. In fact, there are three vortices which are clearly seen in Fig. 3 and slightly masked by the viscosity in Fig. 2. A close examination of Fig. 8 of [1] also indicates the presence of three extra vortices (though the middle one is the most pronounced). In Case B, both our results and Fig. 3 of [2] show the presence of only one extra vortex. It may be

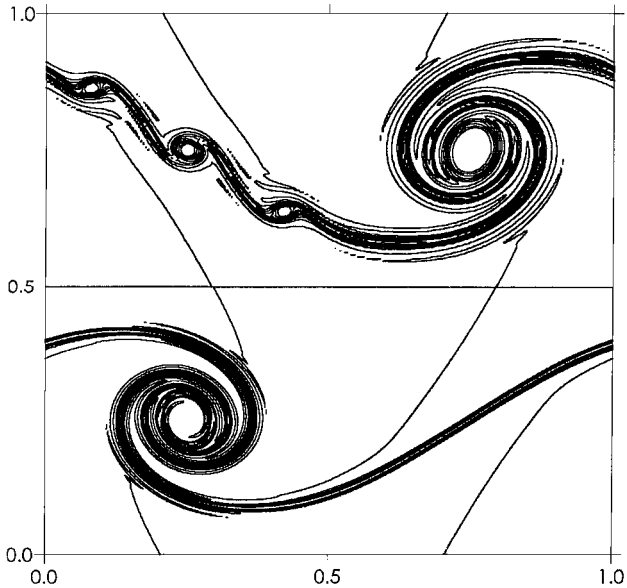

FIG. 3. Removing spurious vortex by refining meshes in the inviscid case: vorticity contours for the thin layer example of [1] with $\mathrm{Re} = \infty$. The meshes are 257×257 (top) and 513×513 (bottom).

explained by the fact that the other two seen in Fig. 4 are sufficiently close to the main vortices to be merged with them by the action of viscous forces.

Based on the above viscous–inviscid results, the following simplified scenario may be suggested. In the inviscid case, the truncation errors arising from nonlinear term discretization

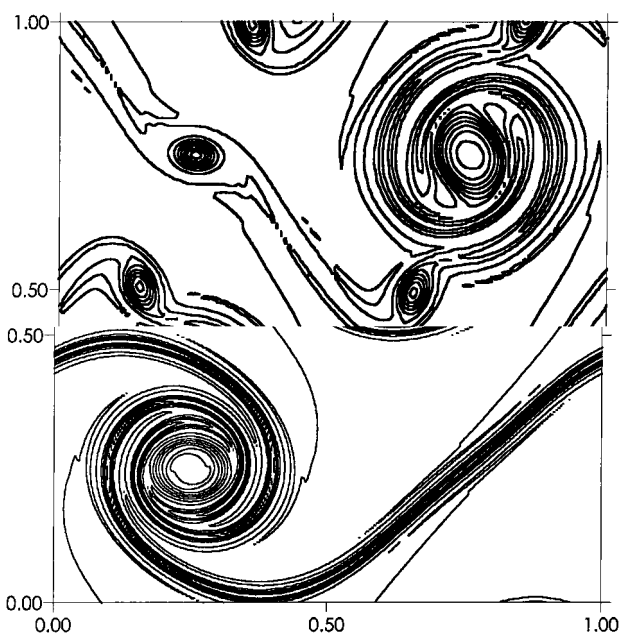

FIG. 4. Removing spurious vortex by refining meshes in the inviscid case: vorticity contours for the thin layer example of [2] with $\mathrm{Re} = \infty$. The meshes are 129×129 (top) and 257×257 (bottom).

(more precisely, their parts with skew-symmetric CUD components) are responsible for producing the artifacts. Despite the presence of high-order derivatives, those errors may be viewed as forcing terms playing the role of small non-singular perturbations to the Euler equations in our double-periodic case (a similar suggestion was formulated in [2]). Due to the unstable nature of the thin shear layers, they provoke considerable changes in numerical solutions. In general, these changes may depend on the layer parameters and initial perturbations. In the case of (2a) and (2b), there are three extra vortices.

When meshes are refined, the magnitude of the vorticity-producing parts of the forcing terms rapidly decreases (as $O(h^6)$ for the present CUD method, where h is the mesh size). For some h, they become negligible when compared with the $O(h^5)$ dissipative terms due to the self-adjoint CUD components and $O(h^4)$ truncation errors introduced by the Laplace operator, and the ψ-derivative discretizations (which are assumed to be non-vorticity-producing). As a result, the artifacts became invisible, the most powerful middle vortex being the last to visually disappear.

In the case of the Navier–Stokes equations, the vorticity-producing terms should be compared with $O(1/\mathrm{Re})$ viscous ones, rather than with other high-order parts of the truncation errors. As a result, the viscous terms "kill" the artifacts when coarser meshes than those in the inviscid calculations are used. The reduced number of grid points needed to remove the artifacts in Case B both in CUD and as reported in [2] also fits neatly into the speculations. Indeed, the Re number is two times smaller in this case, thus defining more powerful viscous forces; they remove the artifacts when coarser meshes are used.

Comparisons of the enstrophy decays in the well-resolved case, which confirm certain of the above suggestions, are presented in Fig. 5. As can be seen, the enstrophy decreases far more rapidly in the viscous case, showing that the viscous dissipation considerably outweighs the numerical dissipation introduced by the self-adjoint part of the CUD operator. Hence, the latter is not responsible for the coarser meshes needed to obtaining artifact-free solutions in the present viscous calculations. Theoretically, the CUD dissipation acts only in the domain of the shortest waves supported by grids. It is likely to influence mainly the shear layer thickness rather than the relatively large vortex structures. Therefore, the early disappearance of the spurious effects in the viscous cases may be attributed to the weak intensity of their contributors and the ability of the CUD scheme to operate well under conditions of coarse meshes.

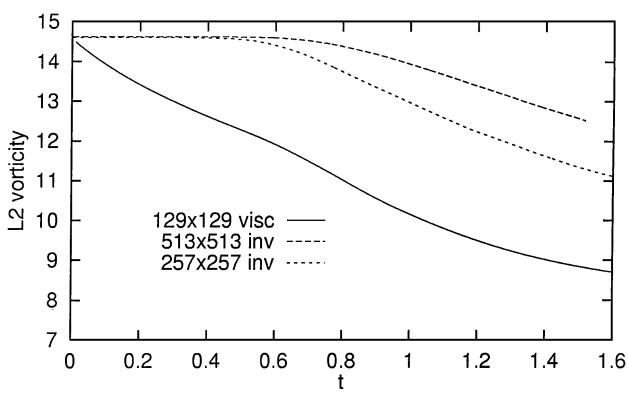

FIG. 5. Vorticity decay curves for the well-resolved viscous and inviscid solutions in Case B.

The behavior of the inviscid decay curves shown in Fig. 5 is worthy of notice. They show almost constant values for $t < t_*(h)$ and tend to go down with time for $t > t_*$ despite the theoretically small numerical dissipation. This may be explained in the following way.

It is well known that norms of deviations of numerical solutions from exact ones are bounded by norms of truncation errors multiplied by "stiffness" factors independent of mesh size, which characterize responses of numerical solutions to input data perturbations. The factors (which, in general, are functions of solutions) may be very large for unstable problems, thus provoking noticeable differences between numerical and exact solutions even in the case of very small truncation errors. In the present conservative scheme, the integral balance is affected mainly by the boundary values. At $t < t_*$, the $y = \text{const}$ boundaries are less disturbed, thus introducing lesser enstrophy losses. As can be expected, the losses for the 513×513 meshes are considerably less than those for the 257×257 meshes. It should be noted that the flow patterns in both cases are indiscernible.

The above reasoning concerning the artifacts' appearance and removal seems to be applicable to other upwind schemes, the difference due only to the magnitudes of truncation errors of the nonlinear terms. For example, Fig. 8 of [1] shows (as has been already mentioned) exactly three spurious vortices in the under-resolved calculations with a dissipative Godunov-type method. One may assume that they can be attributed to the corresponding inviscid pattern produced by the Godunov-type discretization.

4. A more complicated problem seems to be the estimation of the relation between initial perturbations and the vortex-producing ability of schemes in the limit of $\mathrm{Re} = \infty$.

To provide an argument confirming their wavenumber 2 suggestion, the authors of [2] added to the basic initial data (2b) a function which results in a perturbation with twice the frequency of the initial one. The results of calculations [2] showed the existence of an additional "true" vortex midway between the main vortices which does not disappear when meshes are refined (Fig. 9 of [2]). The same picture was obtained with the present method and two times coarser mesh.

However, using (2a) instead of (2b) with the wavenumber 2 perturbation

$$\tilde{u} = \epsilon \cos(4\pi x + 0.25)\cos(2\pi y), \quad \tilde{v} = 2\epsilon \sin(4\pi x + 0.25)\sin(2\pi y), \quad \epsilon = .00375 \tag{3}$$

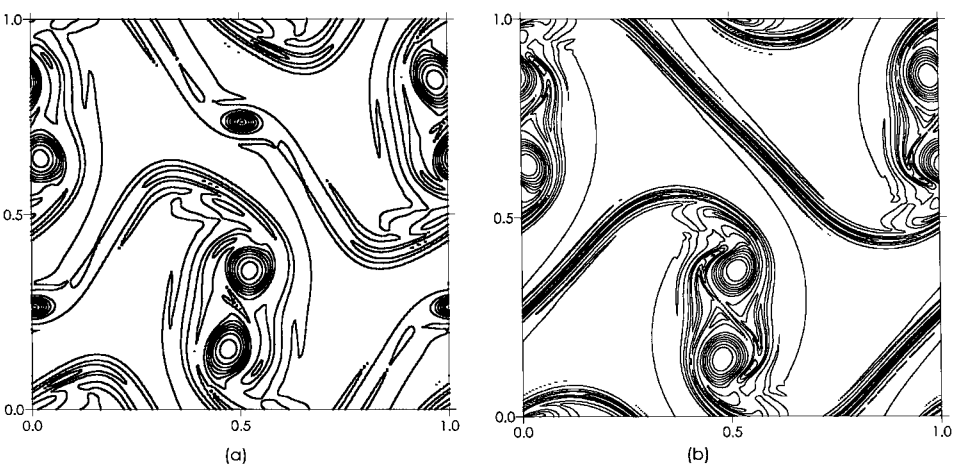

FIG. 6. Results of adding wavenumber 2 perturbation (3) to "main" perturbation (2b) in the inviscid case: vorticity contours for the thin layer parameters [2] with $\mathrm{Re} = \infty$. The meshes are 129×129 (a) and 257×257 (b).

(that is, the combination which was not considered in [2]) was found to produce a quite unexpected vortex configuration. In the inviscid case, the main double-vortex pattern was accompanied by a spurious midway vortex in the under-resolved results. The latter disappeared when meshes were refined to give the double-vortex structure for which (contours are presented in Fig. 6 for the parameters of Case B and $\mathrm{Re} = \infty$). The Navier–Stokes calculations showed the same mesh-converging solution when coarser meshes were used. Though a wavenumber 2 initial perturbation (3) was added, the pattern shown in the figure has little in common with that obtained for the wavenumber 2 initial data of [2] (see [2], Fig. 9).

Hence, additional studies on the role of initial disturbances are needed. From the practical viewpoint, the open question is to what extent is it possible to reduce the number of grid points corresponding to mesh-converged solutions by further refining difference schemes.

REFERENCES

1. D. L. Brown and M. Minion, Performance of underresolved two-dimensional incompressible flow simulations, *J. Comput. Phys.* **121**, 165 (1995).
2. D. L. Brown and M. Minion, Performance of underresolved two-dimensional incompressible flow simulations II, *J. Comput. Phys.* **137**, 734 (1997).
3. A. I. Tolstykh and M. V. Lipavskii, On performance of methods with third- and fifth-order compact upwind differencing, *J. Comput. Phys.* **140**, 205 (1998).
4. A. I. Tolstykh, Two-step fifth-order methods for evolutionary problems with positive operators, *Positivity* **2**, 193 (1998).